J Nanopart Res (2014) 16:2787
DOI 10.1007/s11051-014-2787-2

RESEARCH PAPER

Magnetic $BaFe_{12}O_{19}$ nanofiber filter for effective separation of Fe_3O_4 nanoparticles and removal of arsenic

Jeehye Byun · Hasmukh A. Patel · Cafer T. Yavuz

Received: 29 July 2014 / Accepted: 1 December 2014 / Published online: 11 December 2014
© Springer Science+Business Media Dordrecht 2014

Abstract Magnetic nanoparticles are promising in applications where magnetic separation is intended, although material losses via leaching mechanisms are often inevitable. Magnetic separations with widely available permanent magnets can effectively trap particles, leading to a complete removal of used or waste particles. In this report, we first demonstrate the synthesis of the thinnest (112.7 ± 16.4 nm) and most magnetic (71.96 emu g^{-1}) barium hexaferrite ($BaFe_{12}O_{19}$, BHF—fridge magnet) via an organic solvent-free electrospinning procedure. When the fibers are then packed into a column, they clearly remove 12 nm magnetite (Fe_3O_4) nanoparticles quantitatively. The same BHF cartridge also removes more than 99.9 % As-treated magnetite nanoparticles at capacities up to 70 times of its weight. As a result, one liter of 150 μg L^{-1} As-contaminated water can be purified rapidly at a material cost of less than 2 US cents.

Keywords Magnetic separation · Barium hexaferrite nanofiber · Iron oxide nanoparticle · Arsenic removal · Environmental and health effects

Electronic supplementary material The online version of this article (doi:10.1007/s11051-014-2787-2) contains supplementary material, which is available to authorized users.

J. Byun · H. A. Patel · C. T. Yavuz (✉)
Graduate School of EEWS, Korea Advanced Institute of Science and Technology (KAIST), Daejeon 305-701, Republic of Korea
e-mail: yavuz@kaist.ac.kr

Introduction

Magnetic nanoparticles (Hao et al. 2010) offer significant advantages in applications where size-dependent properties such as magnetism (Sun et al. 2000) and separation (Yavuz et al. 2009), biomedical transport (Pankhurst et al. 2003) and imaging (Kim et al. 2003), surface adsorption (Yavuz et al. 2006), and plasmon (Shevchenko et al. 2008) matter. Magnetic separation, in particular, relies on the particle sizes and distribution (Mayo et al. 2011; Yavuz et al. 2009). There is an inversely proportional relationship between the size of the particles and the field required to sequester them. Although we reported manageably low fields (e.g. 0.3 T) for separation of nanoparticles with small sizes (Yavuz et al. 2006), the time required for a full capture (>6 min) is too long for continuous stream applications, a usually preferred form for large industries.

Arsenic poses health hazards to humans and aquatic ecosystem if its concentration exceeds permissible limits (Yavuz et al. 2006). The major source of arsenic pollution in the environment is the smelting of ores such as those of gold, silver, copper, and others. Arsenic from these sources is distributed in the air, water, soil and finds its way into the human diet by way of direct inhalation or through contamination of water and consumer products (Jarup 2003). Among the various sources of arsenic, the leaching of arsenic into drinking water poses significant threat to human health (Smedley and Kinniburgh 2002). Arsenic poisoning has become a worldwide epidemic, especially in

developing countries where most of the population depends on ground water for drinking (Jiang 2001). Arsenic is one of the most toxic waterborne contaminant and possesses a serious health risk in many countries of the world by triggering skin, lung, and kidney cancers (Smith et al. 1992). Since the adverse impact of arsenic has been widely reported, its permissible limit has been lowered in many parts of the world. The World Health Organization (WHO) reduced the recommended maximum level of arsenic in drinking water to 10 μg L^{-1} in 1993, and the United States environmental protection agency (EPA) adopted a new maximum contaminant level as 10 μg L^{-1} in 2001 (Smedley and Kinniburgh 2002).

In order to remove the arsenic from contaminated water, various methods have so far been utilized such as coagulation (Cheng et al. 1994), precipitation (Bothe and Brown 1999), ion exchange (Vaaramaa and Lehto 2003), and membrane filtration (Geckeler and Volchek 1996). Among them, adsorption is the most widely used method because it is simple, cost-effective, and sludge free (Patel et al. 2012). To name a few, yttrium carbonate (Wasay et al. 1996), coconut husk carbon (Manju et al. 1998), ferrihydrite (Raven et al. 1998), activated carbon (Pattanayak et al. 2000), zirconium oxide (Suzuki et al. 2001), orange juice residue (Ghimire et al. 2002), immobilized biomass (Kamala et al. 2005), goethite (Lafferty and Loeppert 2005), magnetite nanoparticles (Yavuz et al. 2006), chitosan biosorbent (Boddu et al. 2008), maghemite nanoparticle (Tuutijarvi et al. 2009), graphene oxide (Chandra et al. 2010), and core–shell nanostructured iron oxide (Mou et al. 2011, 2012) are developed for the arsenic removal from aqueous solution. Magnetic nanoparticles have shown great promise as arsenic adsorbents due to their ease of separation from the complex natural systems (Yavuz et al. 2006). Various studies reported the favorable characteristics of the magnetic nanoparticles such as high surface area, durability, resistance to oxidation, less sensibility to organic fouling, and high selectivity toward arsenic compounds (Beker et al. 2010; Mayo et al. 2007; Tang et al. 2011; Yavuz et al. 2010, 2006, 2009; Yean et al. 2005).

Although very effective in arsenic remediation, leaching and slow adsorption by the magnetic nanoparticles are of great concern, especially when nanoparticles are used for water treatment. Therefore, it is necessary to improve separation technologies for nanoparticles. In conventional magnetic separation processes, a strong external magnetic field is compulsory to fully separate the nanoparticles from water and this process incurs high costs from energy-intensive electromagnet and non-continuous permanent magnets. The immobilization of the nanoparticles on the supports has been utilized to prevent leaching; however, the significant loss of surface area hinders the adsorption potential of nanoparticles. A new approach to overcome this loss of efficacy is imminent.

Barium hexaferrites (BHF) received great attention due to their high coercivity, high saturation magnetization, high electric resistance, and excellent chemical stability (Tucek et al. 2010). It is known that the magnetic property of BHF is highly dependent on its size, shape, and homogeneity (Chen et al. 2000) and also reported that magnetic materials in fibrous form could show enhanced magnetic behavior (Goldberg 1988). To the best of our knowledge, BHF fibers, despite of their potential, were never considered in water treatment applications that use magnetic separations. Because BHF is derived from iron oxide, it is expected that they also show affinity toward arsenic. In fact, BHF microparticles show high arsenic adsorption capacity in comparison to the parent iron oxide of similar sizes (Patel et al. 2012).

Herein, we report BHF nanofibers that are produced by a simple electrospinning process, which resulted in the thinnest nanofibers with thickness of 112.7 ± 16.4 nm and the highest saturation magnetization of 71.96 emu g^{-1} to date. The fibers, when packed into a non-magnetic column, are capable of separating 12 nm magnetite nanocrystals quantitatively in a bench-top continuous flow operation. The nanoparticles are also pre-treated with arsenic and fed through the column, leading to a rapid, cost-effective, quantitative removal. The process is found to be low cost, maintenance free, and practical for a point-of-use concept.

Experimental

Materials

All reagents were of analytical reagent grade and were used as supplied. Ferric nitrate nonahydrate ($Fe(NO_3)_3 \cdot 9H_2O$, 98 %), poly (vinyl alcohol) (PVA, M_w = 85,000–124,000, 99 + % hydrolyzed), 1-octadecene,

Igepal® CO-630, arsenic standard solution (1,000 mg L^{-1}), and sodium hydroxide (NaOH, 98 %) were purchased from Sigma-Aldrich, USA. Barium nitrate ($Ba(NO_3)_2$, 98.5 %) and ferric oxyhydroxide (FeO(OH)) were purchased from JUNSEI, Japan. Triton® X-100, oleic acid, hydrochloric acid (35–37 %), acetone (99.5 %), and hexane (96 %) were purchased from SAMCHUN, Republic of Korea. Deionized water (18.3 MΩ cm, Purepower I^+ by Human Corporation) was used for all experiments.

Preparation of the $BaFe_{12}O_{19}$ (BHF) nanofibers

Typically, 1.02 g of ($Fe(NO_3)_3 \cdot 9H_2O$) and 0.0547 g of $Ba(NO_3)_2$ were added to 8.2 g of poly (vinyl alcohol) solution (10 wt%). Triton® X-100 surfactant (0.3 v/w %) was added to the mixture to lower the surface tension of the solution. The viscous solution transferred into a plastic syringe was loaded in the electrospinning equipment. The solution was released at a rate of 0.5 mL h^{-1} using a syringe pump (ESR200RD, NanoNC) with 24 kV of the applied voltage. The as-synthesized fibers were heated up to 550 °C for 3 h with the heating rate of 1 °C min^{-1}, followed by heating up to 800 °C at a rate of 10 °C min^{-1} for 2 h, all in air.

Adsorption, separation, and regeneration studies

Two different sizes of magnetite nanoparticles were prepared for the separation and adsorption studies following literature reports (Yavuz et al. 2006; Zhang et al. 2012): laboratory-prepared magnetite nanoparticles (MagL, 12 nm) and commercially available magnetite nanoparticles (MagC, 50–100 nm) (Figure S1). In a typical separation process, magnetite nanoparticles with or without aqueous arsenic solution treatment passed through a cartridge at a flow of 1 mL min^{-1}, where a polyethylene column was packed with BHF fibers sandwiched between glass wools (Figure S2). All column cartridges contained 10 mg of the nanofibers and enough glass wool with a packing density of about 0.021 g cm^{-3}.

Separation of magnetite nanoparticles

Typically, separation of nanoparticles was conducted with 300 mL of aqueous magnetite solution. 7 mg of MagL nanoparticles (for MagC, 10 mg) was dispersed into 10 mL of deionized water, and the dispersed solution was injected into the BHF column. The filtrate was collected and analyzed by ICP-MS to check iron and barium concentrations. All samples for ICP-MS measurement were digested by dilute nitric acid. The separation efficiency of the magnetite nanoparticles was calculated based upon the concentration of iron in the effluent.

Separation of Arsenic-treated magnetite nanoparticles

Separation of arsenic-treated nanoparticles was conducted in the same system except primary adsorption of arsenic onto magnetite nanoparticles. Pre-adsorption of arsenic onto magnetite nanoparticles was performed with different initial arsenic concentrations of 0.15, 0.42, 1.53, and 6.86 mg L^{-1} in batch procedure at 25 °C. The initial pH value of the aqueous arsenic solution was adjusted to 8.05 ± 0.11 using 1 M NaOH or HCl which is close to the groundwater condition. The arsenic solutions with the adsorbents were equilibrated on a slow rotator with tumbled end-over-end (8 rpm) for 24 h. After 10 mL of the arsenic solution being filtered, the filtrates were tested by ICP-MS to check arsenic removal efficiency. The separation/removal efficiency (%) was calculated as follows:

$$\text{Removal efficiency} = \frac{(C_0 - C_e)}{C_0} \times 100,$$

where C_0 and C_e are the initial and equilibrium concentrations of adsorbates in the aqueous solution.

Regeneration of BHF fiber column

Arsenic solution with the concentration of 0.15 mg L^{-1} was treated using MagL nanoparticles, and 30 mL of the solution was filtered through BHF cartridge. A mild washing was conducted with 10 mL of 0.1 M HNO_3 or 0.1 M NaOH solution to investigate the effect of pH in column regeneration. After washing, the column was fed with another 30 mL of arsenic-treated MagL solution, and the filtrates were analyzed by ICP-MS to check arsenic, iron, and barium concentrations.

Characterization

In order to investigate the morphologies of BHF nanofibers, transmission electron microscopy (TEM,

300 kV, Tecnai G2 F30) and scanning electron microscopy (SEM, Nova 230) were utilized. X-ray diffraction analysis was carried out using multipurpose high power X-ray diffractometer (Rigaku, D/MAX-2500). The quantitative analysis of As, Fe, and Ba contents was measured by inductively coupled plasma mass spectroscopy (ICP–MS, Agilent 7,700 s). Magnetic measurement of annealed BHF fibers was performed on a superconducting quantum interference device magnetometer (SQUID, Quantum Design MPMS-7).

Results

Synthesis and characterization of $BaFe_{12}O_{19}$ nanofibers

Electrospinning is known to be easily employed for large-scale synthesis of nanofibers of desired elemental compositions, phases, and sizes (Huang et al. 2003). BHF nanofibers were generated by electrospinning of the polymeric aqueous solution of iron and barium salts followed by an annealing process. Figure 1 shows that the as-spun BHF nanofibers were poorly crystalline while the XRD pattern of annealed fibers revealed the formation of hexagonal barium ferrite phase. The diffraction peak can easily be indexed to $BaFe_{12}O_{19}$ (JCPDS 84-0757) from the diffraction planes at (101), (102), (006), (110), (008), (112), (107), (114), (200), (203), (205), (206), (217), (303), (304), (2011), (220), (2014), and (317), and the

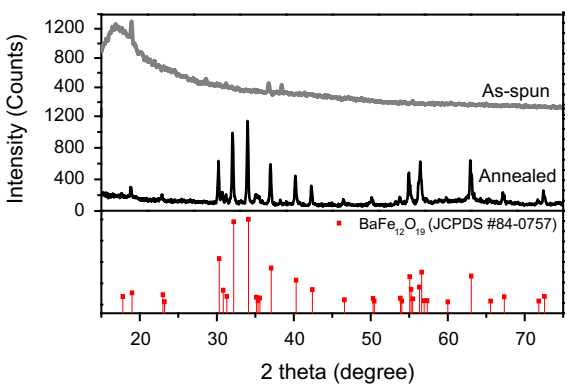

Fig. 1 XRD pattern of as-spun fibers (*gray*) and the annealed nanofibers (*black*) with an indication of $BaFe_{12}O_{19}$ formation (JCPDS #84-0757)

sharp peaks confirmed the products were highly crystalline. The crystallite size of the nanofibers was estimated by Scherrer's equation as follows (Birks and Friedman 1946):

$$\tau = \frac{K\lambda}{\beta \cos \theta},$$

where τ is the mean size of the ordered crystalline domain, K is shape factor (0.94, spherical and cubic), λ is X-ray wavelength (0.15406 nm, CuK_{α}), and β is FWHM in radian. The least squares fitting residual (R) was 9.35 % which should be generally less than 10 %. The estimated mean crystallite size was found to be 57.6 nm which is smaller than the morphological grain size revealed from the micrographs. Figure 2a displays a photograph of nanofibers. The as-spun nanofibers were yellowish in color, which turned brown during calcination at 800 °C. The annealed fibers show high affinity toward external magnetic fields. Field emission scanning electron micrographs (FE–SEM) of as-synthesized and annealed BHF nanofibers show that there is no disruption in length of the nanofibers though reduction in thickness is visible. The latter could be due to the removal of polymeric matrix during calcinations (Fig. 2b, c).

Transmission electron microscope (TEM) images reveal the string of pearl-like morphology (Fig. 3a). The unidirectional structure with an average thickness of 112.7 ± 16.4 nm was observed (the thickness was calculated by averaging the widest points of the grains), one of the thinnest BHF nanofibers ever reported (Fig. 3b). When compared to the calculated size from Scherrer's equation (57.6 nm), the fibers are nearly twice as thick as the crystallites. Considering continuous blob-like attachment of BHF particulates, condensation of the metal oxide surfaces of individual BHF crystals seems to be the most plausible mechanism. High-resolution TEM confirmed the formation of single crystalline phases structure with lattice spacing of 0.386 nm which corresponds to (006) plane of $BaFe_{12}O_{19}$ phase (Fig. 3c). The chemical composition of BHF was confirmed by energy-dispersive X-ray spectroscopy (EDX) and scanning TEM (STEM) mapping analysis (Fig. 3d). The EDX mapping images show that Ba, Fe, and O are well distributed throughout the nanofibers. Quantitative atomic ratio of EDX spectrum between Fe and Ba was 12.35, which is almost identical to the theoretical ratio of $BaFe_{12}O_{19}$. The matrix, poly(vinyl alcohol)–PVA,

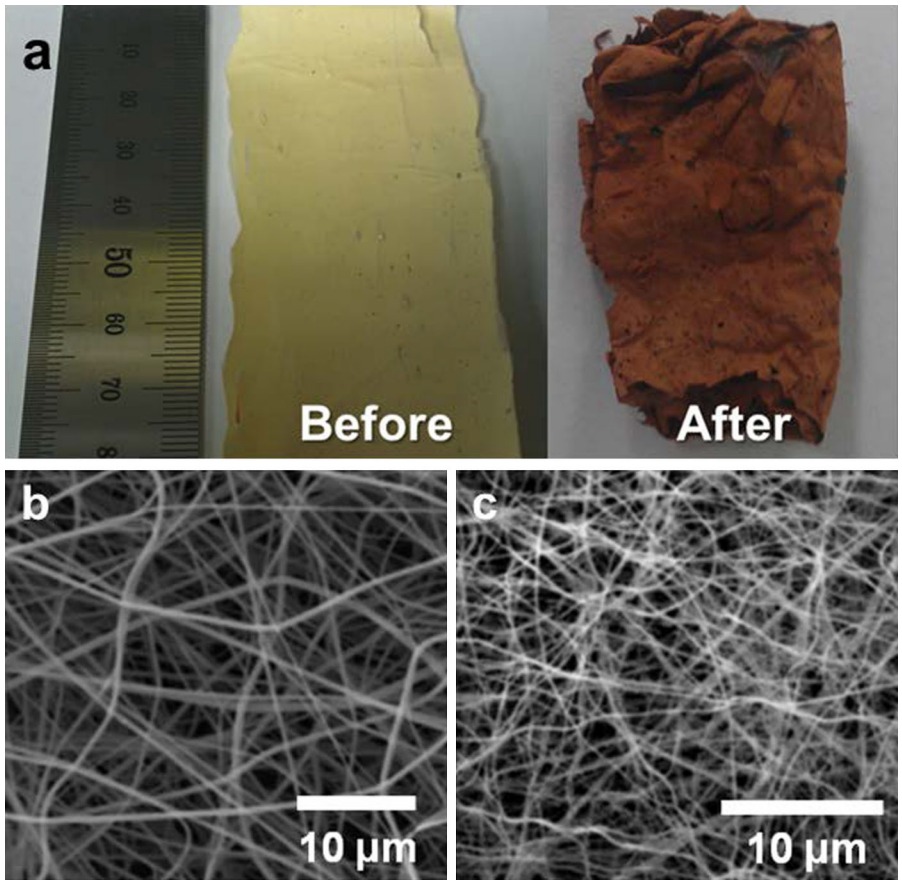

Fig. 2 **a** Photographs of nanofibers before and after heat treatment. SEM morphologies of **b** as-spun nanofibers and **c** the annealed nanofibers

is known for its high surface tension resulting from high degree of hydrolysis, and thus high critical field is necessary to electrospin PVA-containing nanofibers (Finch 1973). One approach is to use non-ionic surfactants (e.g. Triton® X–100) at concentrations as low as 0.3 % v/w (Yao et al. 2003) in order to minimize the formation of droplets and reduce the thickness of nanofibers (Lee et al. 2004). The BHF nanofibers synthesized without Triton® X–100 show an average thickness of 163.3 ± 23.6 nm, 1.5 times larger than synthesis with a surfactant (Figure S3).

The magnetic properties of the BHF nanofibers were investigated using SQUID at 300 K (Fig. 4). The coercivity (H_c) and saturated magnetization (M_s) of BHF nanofibers is 2,568 Oe and 71.96 emu g^{-1}, respectively. To the best of our knowledge, M_s value is the highest reported to date. Typically, various values of H_c (2,952–6,400 Oe) and M_s (17.8–71.5 emu g^{-1}) of hexagonal $BaFe_{12}O_{19}$ powders (Benito et al. 2001; Huang et al. 2003; Mohsen 2010), hollow fibers (Mou et al. 2010), and electrospun fibers (Liu et al. 2012; Zhang et al. 2012) have been reported (Table S1). The BHF nanofibers reported here exhibit low H_c and high M_s mainly because of their small dimensions. High M_s of nanofibers results from the high purity, single crystallinity, and small sizes of nanofibers, which are consistent with the XRD and TEM measurements. The critical single-domain radius of $BaFe_{12}O_{19}$ was calculated to be 290 nm (Skomski 2003), which is higher than the experimental crystallite size of the BHF nanofibers, suggesting that the fibers act like uniform domain state(Chen et al. 2000), although there is room for further experimental verification. Moreover, the squareness ratio (M_r/M_s) is about 0.5, which is close to the expected value for randomly packed single-domain particles when a coherent magnetization

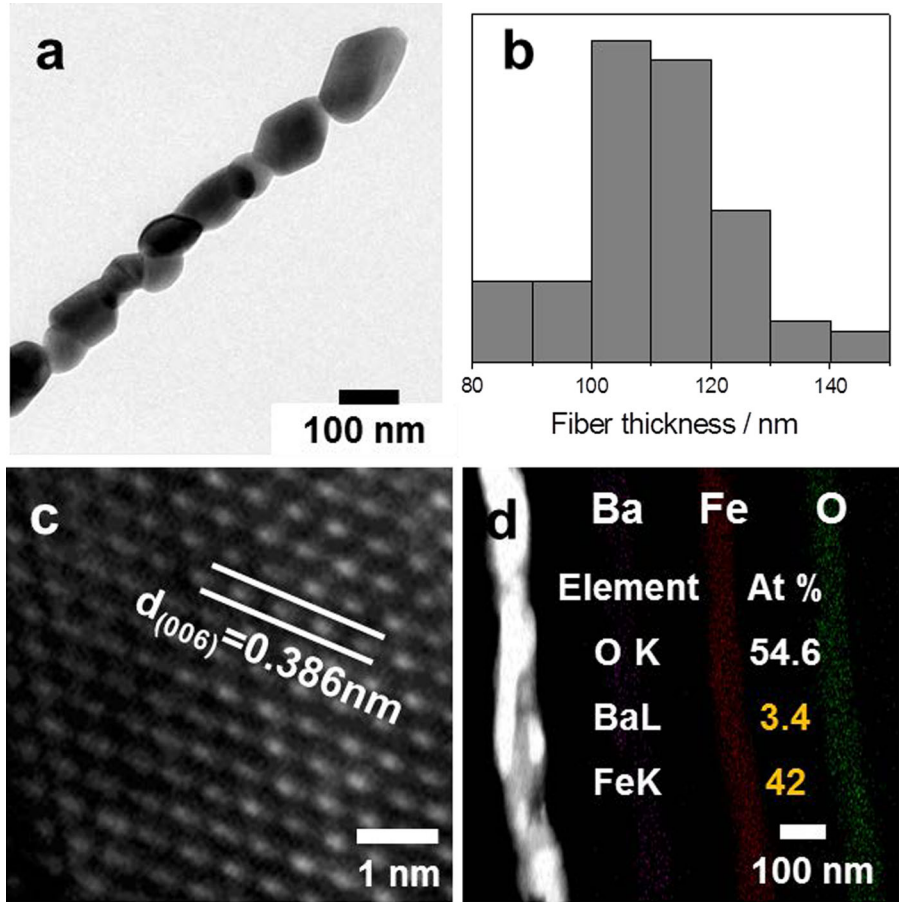

Fig. 3 **a** TEM morphology of nanofibers and **b** their thickness distribution ($N = 200$). **c** HRTEM image of a blob of fiber with lattice spacing measurement. **d** EDX mappings with quantitative analysis of the spectra

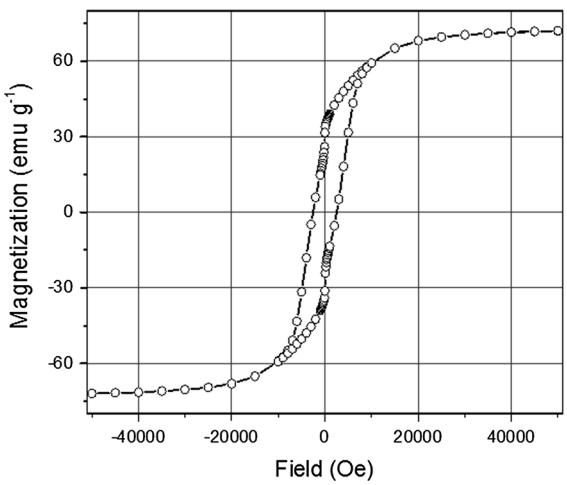

Fig. 4 Magnetic hysteresis loop of nanofibers measured at 300 K

rotation reversal mechanism is hypothesized (Benito et al. 2001). For the single-domain ferrites, it is well known that the H_c decreases as the crystallite size decreases due to the randomizing effects of thermal energy (Batlle et al. 1993; Chen and Chen 2001; Rezlescu et al. 1999). Therefore, it is believed that the single-domain nanofibers with small crystallites show lower H_c.

Magnetic separation of nanoparticles via BHF fiber cartridge

Magnetite nanoparticles are widely considered to be an effective absorbent for the As removal from contaminated water (Cumbal and Sengupta 2005; DeMarco et al. 2003; Mayo et al. 2007; Mohan and Pittman 2007; Mou et al. 2011, 2012; Yavuz et al. 2010, 2006, 2009; Yean et al. 2005); however, their separation after treatment remains costly, especially because of the need for strong, rare-earth magnets. The BHF nanofibers could resolve this problem because (1) they are very inexpensive (also known as fridge

magnets) and (2) by weaving fibers into nets for a cartridge application would eliminate the use of magnets due to the fact that incoming stream would have high contact surface and proximity. First of all, magnetic separation of nanoparticles was tested by the filtration of magnetite solution through the column packed with BHF nanofibers.

In order to evaluate the capacity of magnetic separation, 300 mL of magnetite solutions with two different sizes (210 mg for MagL, 300 mg for MagC) were passed through the BHF nanofiber cartridge, and concentration of the filtrate was monitored by ICP–MS at periodic intervals. The color of filtrate is visually transparent after being passed through the BHF column. Figure 5a shows separation efficiency of nanoparticles and residual concentration of magnetite in the filtrate. For 12-nm-sized MagL nanoparticles, the concentration was found to be a maximum of 0.17 mg L^{-1} up to 50 mL and decreased below 0.02 mg L^{-1} afterward, much less than the acceptable limit of iron (up to 3 mg L^{-1}) throughout the measurement(Fawell et al. 2003). For MagC nanoparticles with much larger size, the maximum concentration was only 0.4 μg L^{-1}, indicating a perfect separation of nanoparticles from water. Moreover, the total amount of MagL and MagC in 300 mL effluent was about 0.0038 mg and 0.039 μg, respectively, demonstrating that more than 99.99 % of the nanoparticles were retained in the column (Table S2 for the details). The concentration of magnetite remained fairly marginal even though the amount of injected nanoparticles increased. The average concentration of barium in the filtrate ranged from 0.02 to 0.03 mg L^{-1} in both of MagC and MagL, which is also much less than the drinking water standard of barium, up to 2 mg L^{-1}(Wones et al. 1990). The complete separation of the nanoparticles is attributed to the magnetic interaction between the BHF nanofibers and magnetite nanoparticles, where magnetically induced aggregation of magnetite on top of the BHF fibers was observed. The aggregates not only make the pores of cartridge smaller but also promote further magnetic interaction of the incoming particles, leading to an enhanced separation. In order to assess the upper limit for nanoparticle removal capacity of the fibers, a high concentrated MagL solution, 700 mg with 100 mL aqueous solution, was filtered through the cartridge (Figure S4). The MagL concentration in the effluent was ranged from 2.4 to 6.4 ppm, and the total amount of magnetite in 100 mL was about 5.38 mg, showing that 99.23 % of the nanoparticles was separated. With the high loading of the nanoparticles, however, the flow of the solution started to slow down when 280 mg of MagL equivalent was loaded and stopped at 700 mg equivalent of injection. Therefore, the total capacity of BHF filter cartridge was determined to be 700 mg MagL per 10 mg BHF, indicating that the nanofibers could carry a maximum of 70 times their weight. In practical systems, however, the maximum capacity is expected to go up since the loading capacities with 70-mg aliquots are expected to be lower because of the concerted reversible aggregation of nanoparticles among themselves (Yavuz et al. 2006). For field operations, a safe upper limit of 250 mg (25 times more weight than the BHF used in the cartridge) can be advised in a consideration of injection speed.

SEM image of BHF nanofibers exhibits that the fibers do not show change in length after separating 300 mL of magnetite solution (Fig. 5b). TEM images of BHF nanofibers taken after magnetite separation clearly show that magnetite nanoparticles are attached to the BHF nanofibers, suggesting the locations of captured particles (Fig. 5c, d). The EDX spectrums on the point 1 showed the presence of only Fe content, while the point 2 consisted of both Fe and Ba, further confirming the interactions between the BHF nanofibers and the magnetite nanoparticles.

Removal of arsenic via simple filtration

In order to verify arsenic removal efficiency of the proposed system, two successive adsorptions are necessary (Fig. 6): (i) primary adsorption of arsenic onto magnetite nanoparticles and (ii) secondary adsorption of As-treated magnetite nanoparticles by magnetic separation through BHF nanofiber filter. The initial pH of aqueous arsenic solution was adjusted to 8.0 simulating groundwater conditions (Yean et al. 2005), and also it has been reported that maximum arsenic adsorption capacity of magnetite is attained at about pH 8 since the point of zero charge for magnetite is at pH 6.5 (Su and Puls 2008).

The initial arsenic concentration for adsorption test ranged from 0.15 to 6.86 mg L^{-1} because the concentration of naturally occurring arsenic is about 0.1–1 mg L^{-1} (Bissen and Frimmel 2003), and the maximum permissible limit of arsenic in drinking

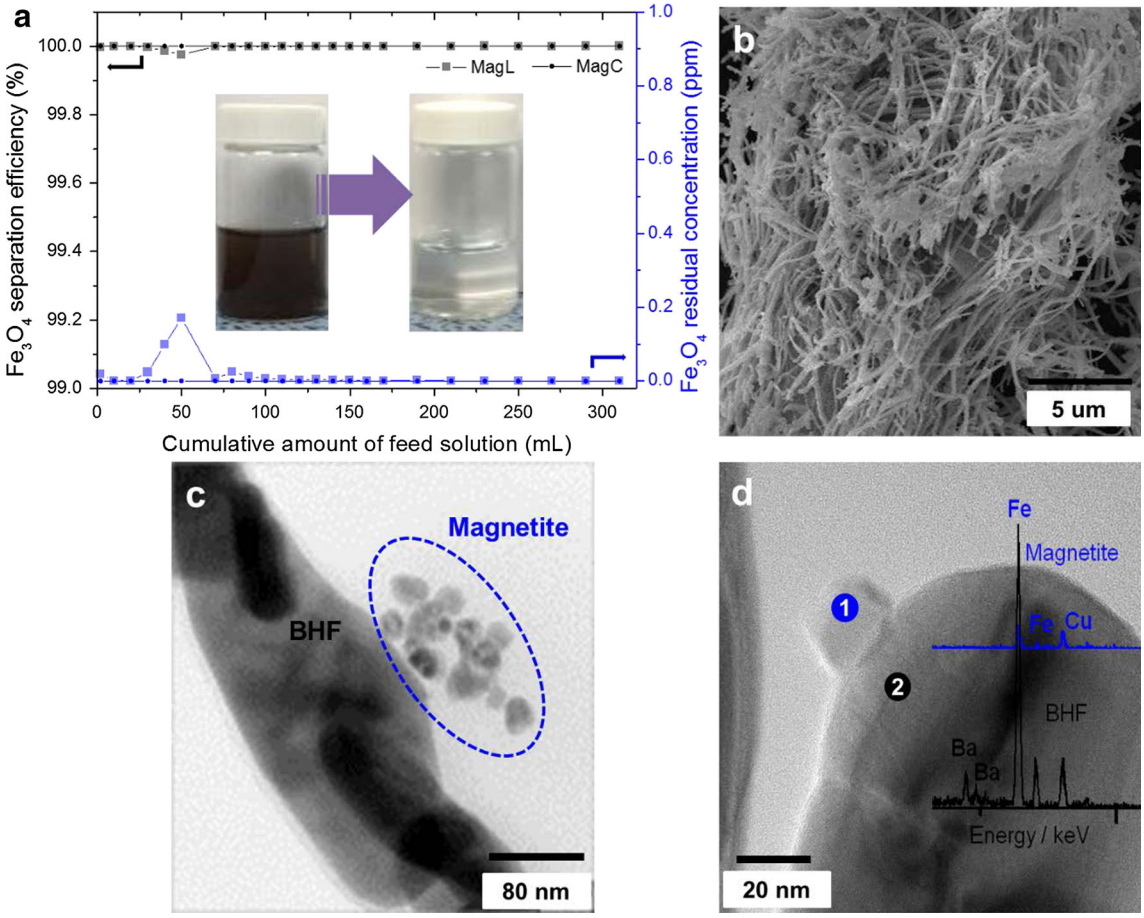

Fig. 5 **a** Separation efficiency of nanoparticles (*black*) and the residual concentration of magnetite in filtrate (*blue*). *Inset* displays photographs of initial feed solution of MagL and its final filtrate. **b** SEM image shows that BHF nanofibers are mostly intact after separating 300 mL of MagL solution. **c** TEM image of BHF and MagL (magnetite) nanoparticle after filtration of 300 mL of MagL solution. **d** EDX spectrum of the TEM image confirms the interaction between BHF and MagL

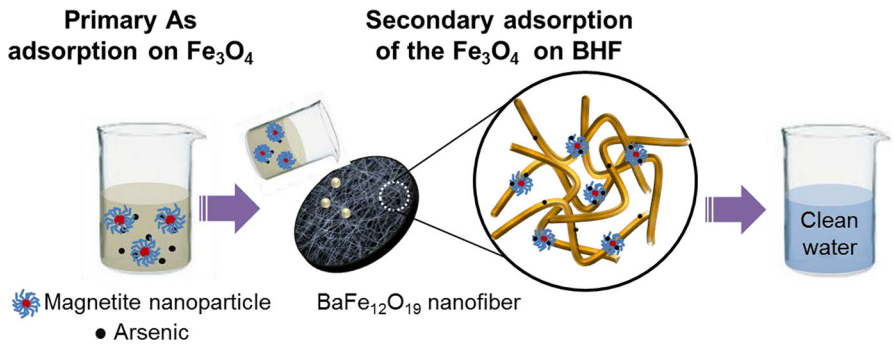

Fig. 6 Schematic illustration of magnetic separation via hybrid adsorption processes

water is 0.01 mg L^{-1} (Vahter 2008). Higher concentrations are intended to see how much capacity the system can handle at the most extreme contamination levels. Figure 7 displays the arsenic removal efficiency of MagL and MagC with the filtration through BHF column. Each 10 mL of arsenic solution in

different concentrations was treated with nanoparticles and passed via BHF cartridge. The overall As removal efficiency with MagL and BHF combination is more than 99 % below 1.5 mg L^{-1} concentrations proving its wide applicability in natural systems. The efficacy of MagL and BHF system, however, decreased down to 84.7 % at 6.86 mg L^{-1}, indicating that quantitative arsenic removal capacity is somewhere below that concentration. For MagC and BHF system, the efficiency recorded about 85 % below 1.5 mg L^{-1} concentrations and decreased down to 70 % at 6.86 mg L^{-1}. At the concentration of 0.15 mg L^{-1}, which is the range of naturally occurring arsenic, MagL and BHF system capture 99.9 % of arsenic from water so that the residual concentration of arsenic recorded only 0.15 μg L^{-1}, well corresponding to the drinking water requirement of the WHO (10 μg L^{-1})(Vahter 2008). The BHF nanofibers themselves were also tested for arsenic removal study in a batch system, 10 mg of the nanofibers being utilized for 24 h of interaction as usual, and a maximum of 45.3 % arsenic was removed in 5.42 mg L^{-1} of As solution. This indicates that BHF nanofibers are also attributed to the high adsorption of arsenic in the hybrid system.

In order to verify the removal of arsenic with the assistance from magnetic separation of MagL, we employed non-magnetic titanium dioxide (TiO_2) nanoparticle, a well-known adsorbent for arsenic treatment (Dutta et al. 2004) and tested it for arsenic removal in the same adsorption conditions. The TiO_2 nanoparticles were treated with the aqueous arsenic solution having different initial concentrations from 0.1 to 6.1 mg L^{-1} and filtered through the BHF nanofiber filter. The color of filtrate through BHF fiber column was found to be opaque due to the presence of TiO_2 nanoparticles (Figure S5). The arsenic removal efficiency with TiO_2 system was 34 % at 0.1 mg L^{-1} and 11 % at 6.1 mg L^{-1}, which is far below than both of MagL and MagC systems. The TiO_2 nanoparticles showed good As adsorption ability when the particles were separated via centrifugation (Dutta et al. 2004); however, the arsenic removal efficiency after filtration through BHF fiber column was just above 10 %. This indicates that arsenic-bound TiO_2 nanoparticles were passing through the BHF filter instead of staying in the column due to non-magnetic interaction between the TiO_2 and BHF nanofiber, finally leading to high arsenic concentration in the filtrate.

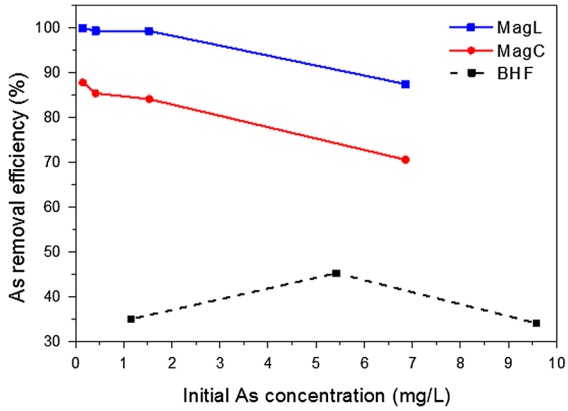

Fig. 7 Arsenic removal efficiency of the solutions treated with MagL (*blue*) and MagC (*red*). The nanoparticles are further filtered through BHF nanofiber column for magnetic separation. *Black square marker* indicates arsenic removal efficiency of BHF fiber itself tested in a separate batch system

Regeneration of BHF fiber column

Regeneration of the BHF filter cartridge with MagL nanoparticles was conducted in different pH conditions (Table S3). After 30 mL of the arsenic solution with MagL nanoparticles was injected into the column, the column was washed and fed with another 30 mL of MagL solution. The reason to use only 30 mL of solution is that there is high probability of nanoparticle leaching in the early stage of injections. After the magnetite with arsenic solution, with the concentration of 0.15 mg L^{-1}, was injected into the BHF column, there occurs high arsenic and magnetite separation with scant concentration of barium. With a mild washing with 10 mL of 0.1 M HNO_3 solution, it had been shown that 7.88 % of arsenic is recovered and second feed after the regeneration revealed that arsenic removal efficiency is slightly increased. However, the BHF nanofibers were affected by the treatment with acidic solution so that the barium concentration both in washing solution and the filtrate after regeneration had elevated. When the column was treated with 10 mL of 0.1 M NaOH solution, the recovery of arsenic is increased up to 12.25 % and the subsequent filtration after the regeneration showed that arsenic removal efficiency had lessened. The desorption of arsenic is known to be increased with the increasing pH (Yean et al. 2005) and the arsenic bound onto the nanoparticles was preferably desorbed in

alkaline solution. Due to the influence of alkaline solutions, arsenic contents were leached out from the column after regeneration, slightly decreasing successive arsenic removal efficiency. On the contrary to the regeneration with acidic solution, the barium concentration was unchanging. The recovery of magnetite nanoparticles was insignificant both in acid and alkaline solutions, and the leaching concentration of the arsenic and barium only altered in different pH conditions.

Socio-economic analysis

The most arsenic affected area is situated in Southeast Asia, more particularly Bangladesh. The arsenic concentration of seven rivers in Bangladesh was found to be in the range of 0.5–29 μg L^{-1} (Smedley and Kinniburgh 2002). Moreover, As concentration in ground water is very high with more than 27 % of the shallow wells containing about 50 μg L^{-1}. A combination of magnetite nanoparticles and BHF nanofiber cartridges described in this study could be extremely useful for these As-contaminated areas due to its availability, adaptability, and facile operation. It should be imperative to look at socio-economic study while targeting ground level implication of this technology. The cost of magnetic nanoparticles and BHF nanofibers were calculated based on the reagents used in this study (Table S4). One gram of BHF fibers can be produced at a cost of USD 0.462, and kitchen synthesis (Yavuz et al. 2010) can provide 1 g of magnetite nanoparticles at a cost of USD 0.021, leading to an estimated value of USD 19.62 for treating 1 m^3 of 150 μg L^{-1} As-contaminated water. A commercial rare-earth magnet costs USD 2.79 per gram, which could be very costly if widespread distribution is intended. It should also be noted that the cost could go down further with industrial scale-up practices.

Conclusion

In summary, we synthesized magnetic $BaFe_{12}O_{19}$ (BHF) nanofibers with thicknesses of 112.7 ± 16.4 nm and saturation magnetization of 71.96 emu g^{-1}, for their use as cartridge filters in efficiently removing and separating magnetic nanoparticles. Coupling with already established arsenic removal procedures by nano-magnetite (Yavuz et al. 2006), BHF nanofibers can assist in removing arsenic from water 99.7 % at 150 μg L^{-1} with a maximum capacity of 700 mg of magnetic nanoparticles for a 99.9 % recovery. The efficient separation of the nanoparticles and the high As removal efficiency was achieved via a rapid, simple, continuous filtration process, and the low cost of BHF nanofibers allow extensive use of this technology in actual field operations, where point-of-use is the only choice. The BHF fibers reported here can also find good use when fine particles are needed to be magnetically separated (e.g., steel industry wastewater).

Acknowledgments This study was supported by the National Research Foundation of Korea, IWT (NRF-2012-C1AAA001-M1A2A2026588). J.B. thanks the National Research Foundation of Korea for a global Ph.D. fellowship (2013H1A2A1033423).

References

Batlle X, Obradors X, Medarde M, Rodriguezcarvajal J, Pernet M, Valletregi M (1993) Surface spin canting in $BaFe_{12}O_{19}$ fine particles. J Magn Magn Mater 124:228–238

Beker U, Cumbal L, Duranoglu D, Kucuk I, Sengupta AK (2010) Preparation of Fe oxide nanoparticles for environmental applications: arsenic removal. Environ Geochem Health 32:291–296

Benito G, Morales MP, Requena J, Raposo V, Vazquez M, Moya JS (2001) Barium hexaferrite monodispersed nanoparticles prepared by the ceramic method. J Magn Magn Mater 234:65–72

Birks LS, Friedman H (1946) Particle size determination from X-ray line broadening. J Appl Phys 17:687–692

Bissen M, Frimmel FH (2003) Arsenic—a review. Part I: occurrence, toxicity, speciation, mobility. Acta Hydroch Hydrob 31:9–18

Boddu VM, Abburi K, Talbott JL, Smith ED, Haasch R (2008) Removal of arsenic(III) and arsenic(V) from aqueous medium using chitosan-coated biosorbent. Water Res 42:633–642

Bothe JV, Brown PW (1999) Arsenic immobilization by calcium arsenate formation. Environ Sci Technol 33:3806–3811

Chandra V, Park J, Chun Y, Lee JW, Hwang IC, Kim KS (2010) Water-dispersible magnetite-reduced graphene oxide composites for arsenic removal. ACS Nano 4:3979–3986

Chen DH, Chen YY (2001) Synthesis of barium ferrite ultrafine particles by coprecipitation in the presence of polyacrylic acid. J Colloid Interface Sci 235:9–14

Chen MS, Shen ZX, Liu XY, Wang J (2000) Raman and magnetization studies of barium ferrite powder prepared by water-in-oil microemulsion. J Mater Res 15:483–487

Cheng RC, Wang HC, Beuhler MD (1994) Enhanced coagulation for arsenic removal. J Am Water Works Assoc 86:79–90

Cumbal L, Sengupta AK (2005) Arsenic removal using polymer-supported hydrated iron (III) oxide nanoparticles: role

of Donnan membrane effect. Environ Sci Technol 39:6508–6515

DeMarco MJ, Sengupta AK, Greenleaf JE (2003) Arsenic removal using a polymeric/inorganic hybrid sorbent. Water Res 37:164–176

Dutta PK, Ray AK, Sharma VK, Millero FJ (2004) Adsorption of arsenate and arsenite on titanium dioxide suspensions. J Colloid Interface Sci 278:270–275

Fawell JK, Lund U, Mintz B, Galal-Gorchev H, Helmer R, Bonnefoy X, Espinoza O (2003) Guidelines for drinking-water quality—iron in drinking-water. World Health Organization, Geneva

Finch CA (1973) Poly(vinyl alcohol): properties and applications. Wiley, London

Geckeler KE, Volchek K (1996) Removal of hazardous substances from water using ultrafiltration in conjunction with soluble polymers. Environ Sci Technol 30:725–734

Ghimire KN, Inoue K, Makino K, Miyajima T (2002) Adsorptive removal of arsenic using orange juice residue. Sep Sci Technol 37:2785–2799

Goldberg HA (1988) High magnetic permeability composites containing fibers with ferrite fill. US Patent No. 4,725,490

Hao R, Xing RJ, Xu ZC, Hou YL, Gao S, Sun SH (2010) Synthesis, functionalization, and biomedical applications of multifunctional magnetic nanoparticles. Adv Mater 22:2729–2742

Huang JG, Zhuang HR, Li WL (2003) Synthesis and characterization of nano crystalline $BaFe_{12}O_{19}$ powders by low temperature combustion. Mater Res Bull 38:149–159

Jarup L (2003) Hazards of heavy metal contamination. Br Med Bull 68:167–182

Jiang JQ (2001) Removing arsenic from groundwater for the developing world—a review. Water Sci Technol 44:89–98

Kamala CT, Chu KH, Chary NS, Pandey PK, Ramesh SL, Sastry ARK, Sekhar KC (2005) Removal of arsenic(III) from aqueous solutions using fresh and immobilized plant biomass. Water Res 39:2815–2826

Kim DK, Mikhaylova M, Wang FH, Kehr J, Bjelke B, Zhang Y, Tsakalakos T, Muhammed M (2003) Starch-coated superparamagnetic nanoparticles as MR contrast agents. Chem Mater 15:4343–4351

Lafferty BJ, Loeppert RH (2005) Methyl arsenic adsorption and desorption behavior on iron oxides. Environ Sci Technol 39:2120–2127

Lee JS, Choi KH, Do GH, Kim SS, Chun DH, Kim HY, Lyoo WS (2004) Role of molecular weight of atactic poly(vinyl alcohol) (PVA) in the structure and properties of PVA nanofabric prepared by electrospinning. J Appl Polym Sci 93:1638–1646

Liu JJ, Gong CR, Fan GL (2012) Preparation and properties of barium-ferrite-containing glass ceramic fibers via an electrospinning/sol–gel process. J Sol-Gel Sci Technol 61:185–191

Manju GN, Raji C, Anirudhan TS (1998) Evaluation of coconut husk carbon for the removal of arsenic from water. Water Res 32:3062–3070

Mayo JT, Yavuz CT, Yean S, Cong LL, Shipley H, Yu WW, Falkner JC, Kan A, Tomson M, Colvin VL (2007) The effect of nanocrystalline magnetite size on arsenic removal. Sci Technol Adv Mat 8:71–75

Mayo JT, Lee SS, Yavuz CT, Yu WW, Prakash A, Falkner JC, Colvin VL (2011) A multiplexed separation of iron oxide nanocrystals using variable magnetic fields. Nanoscale 3:4560–4563

Mohan D, Pittman CU (2007) Arsenic removal from water/wastewater using adsorbents—a critical review. J Hazard Mater 142:1–53

Mohsen Q (2010) Barium hexaferrite synthesis by oxalate precursor route. J Alloy Compd 500:125–128

Mou FZ, Guan JG, Sun ZG, Fan XA, Tong GX (2010) In situ generated dense shell-engaged Ostwald ripening: a facile controlled-preparation for $BaFe_{12}O_{19}$ hierarchical hollow fiber arrays. J Solid State Chem 183:736–743

Mou FZ, Guan JG, Xiao ZD, Sun ZG, Shi WD, Fan XA (2011) Solvent-mediated synthesis of magnetic Fe_2O_3 chestnut-like amorphous-core/gamma-phase-shell hierarchical nanostructures with strong As(V) removal capability. J Mater Chem 21:5414–5421

Mou FZ, Guan JG, Ma HR, Xu LL, Shi WD (2012) Magnetic iron oxide chestnut like hierarchical nanostructures: preparation and their excellent arsenic removal capabilities. ACS Appl Mater Interface 4:3987–3993

Pankhurst QA, Connolly J, Jones SK, Dobson J (2003) Applications of magnetic nanoparticles in biomedicine. J Phys D Appl Phys 36:R167–R181

Patel HA, Byun J, Yavuz CT (2012) Arsenic removal by magnetic nanocrystalline barium hexaferrite. J Nanopart Res 14:881–887

Pattanayak J, Mondal K, Mathew S, Lalvani SB (2000) A parametric evaluation of the removal of As(V) and As(III) by carbon-based adsorbents. Carbon 38:589–596

Raven KP, Jain A, Loeppert RH (1998) Arsenite and arsenate adsorption on ferrihydrite: kinetics, equilibrium, and adsorption envelopes. Environ Sci Technol 32:344–349

Rezlescu L, Rezlescu E, Popa PD, Rezlescu N (1999) Fine barium hexaferrite powder prepared by the crystallisation of glass. J Magn Magn Mater 193:288–290

Shevchenko EV, Bodnarchuk MI, Kovalenko MV, Talapin DV, Smith RK, Aloni S, Heiss W, Alivisatos AP (2008) Gold/iron oxide core/hollow-shell nanoparticles. Adv Mater 20:4323–4329

Skomski R (2003) Nanomagnetics. J Phys Condens Mat 15:R841–R896

Smedley PL, Kinniburgh DG (2002) A review of the source, behaviour and distribution of arsenic in natural waters. Appl Geochem 17:517–568

Smith AH, Hopenhaynrich C, Bates MN, Goeden HM, Hertzpicciotto I, Duggan HM, Wood R, Kosnett MJ, Smith MT (1992) Cancer risks from arsenic in drinking-water. Environ Health Perspect 97:259–267

Su CM, Puls RW (2008) Arsenate and arsenite sorption on magnetite: relations to groundwater arsenic treatment using zerovalent iron and natural attenuation. Water Air Soil Pollut 193:65–78

Sun SH, Murray CB, Weller D, Folks L, Moser A (2000) Monodisperse FePt nanoparticles and ferromagnetic FePt nanocrystal superlattices. Science 287:1989–1992

Suzuki TM, Tanco ML, Tanaka DAP, Matsunaga H, Yokoyama T (2001) Adsorption characteristics and removal of oxo-anions of arsenic and selenium on the porous polymers

loaded with monoclinic hydrous zirconium oxide. Sep Sci Technol 36:103–111

Tang WS, Li Q, Li CF, Gao SA, Shang JK (2011) Ultrafine alpha-Fe_2O_3 nanoparticles grown in confinement of in situ self-formed "cage" and their superior adsorption performance on arsenic(III). J Nanopart Res 13:2641–2651

Tucek J, Zboril R, Namai A, Ohkoshi S (2010) Epsilon-Fe_2O_3: an advanced nanomaterial exhibiting giant coercive field, millimeter-wave ferromagnetic resonance, and magnetoelectric coupling. Chem Mater 22:6483–6505

Tuutijarvi T, Lu J, Sillanpaa M, Chen G (2009) As(V) adsorption on maghemite nanoparticles. J Hazard Mater 166:1415–1420

Vaaramaa K, Lehto J (2003) Removal of metals and anions from drinking water by ion exchange. Desalination 155:157–170

Vahter M (2008) Health effects of early life exposure to arsenic. Basic Clin Pharmacol 102(2):204–211

Wasay SA, Haron MJ, Uchiumi A, Tokunaga S (1996) Removal of arsenite and arsenate ions from aqueous solution by basic yttrium carbonate. Water Res 30:1143–1148

Wones RG, Stadler BL, Frohman LA (1990) Lack of effect of drinking-water barium on cardiovascular risk-factors. Environ Health Perspect 85:355–359

Yao L, Haas TW, Guiseppi-Elie A, Bowlin GL, Simpson DG, Wnek GE (2003) Electrospinning and stabilization of fully hydrolyzed poly(vinyl alcohol) fibers. Chem Mater 15:1860–1864

Yavuz CT, Mayo JT, Yu WW, Prakash A, Falkner JC, Yean S, Cong LL, Shipley HJ, Kan A, Tomson M, Natelson D, Colvin VL (2006) Low-field magnetic separation of monodisperse Fe_3O_4 nanocrystals. Science 314:964–967

Yavuz CT, Prakash A, Mayo JT, Colvin VL (2009) Magnetic separations: from steel plants to biotechnology. Chem Eng Sci 64:2510–2521

Yavuz CT, Mayo JT, Suchecki C, Wang J, Ellsworth AZ, D'Couto H, Quevedo E, Prakash A, Gonzalez L, Nguyen C, Kelty C, Colvin VL (2010) Pollution magnet: nanomagnetite for arsenic removal from drinking water. Environ Geochem Health 32:327–334

Yean S, Cong LL, Yavuz CT, Mayo JT, Yu WW, Kan AT, Colvin VL, Tomson MB (2005) Effect of magnetite particle size on adsorption and desorption of arsenite and arsenate. J Mater Res 20:3255–3264

Zhang JL, Fu JC, Li FS, Xie EQ, Xue DS, Mellors NJ, Peng Y (2012) $BaFe_{12}O_{19}$ single-particle-chain nanofibers: preparation, characterization, formation principle, and magnetization reversal mechanism. ACS Nano 6:2273–2280